Wavefunction statistics and multifractality at the spin quantum Hall transition

A D Mirlin[1,2,3]**, F Evers**[1] **and A Mildenberger**[1]

[1] Institut für Nanotechnologie, Forschungszentrum Karlsruhe, 76021 Karlsruhe, Germany
[2] Institut für Theorie der Kondensierten Materie, Universität Karlsruhe, 76128 Karlsruhe, Germany

Abstract
The statistical properties of wavefunctions at the critical point of the spin quantum Hall transition are studied. The main emphasis is put on the determination of the spectrum of multifractal exponents Δ_q governing the scaling of moments $\langle |\psi|^{2q} \rangle \sim L^{-qd-\Delta_q}$ with the system size L and the spatial decay of wavefunction correlations. Two- and three-point correlation functions are calculated analytically by means of mapping onto the classical percolation, yielding the values $\Delta_2 = -1/4$ and $\Delta_3 = -3/4$. The multifractality spectrum obtained from numerical simulations is given with a good accuracy by the parabolic approximation $\Delta_q \simeq q(1-q)/8$, but shows detectable deviations. We also study statistics of the two-point conductance g, in particular, the spectrum of exponents X_q characterizing the scaling of the moments $\langle g^q \rangle$. Relations between the spectra of critical exponents of wavefunctions (Δ_q), conductances (X_q) and Green functions at the localization transition with a critical density of states are discussed.

PACS number: 73.43.−f

1. Introduction

In the framework of the random matrix theory pioneered by Wigner [1] and Dyson [2], the statistical properties of spectra of complex systems are described by random matrix ensembles. Within the Dyson classification, three symmetry classes are distinguished (orthogonal, symplectic and unitary), depending on whether the system is invariant under the time-reversal transformation and on its spin. It has been understood that this classification is very general and applies to a great variety of physically distinct systems (see [3] for a recent review).

[3] Also at: Petersburg Nuclear Physics Institute, 188350 St Petersburg, Russia.

While the Dyson classification is complete for the bulk of the spectrum, more symmetry classes may arise in the vicinity of a special point on the energy axis. Such non-standard symmetry classes have attracted a considerable research attention during the last decade. One group of them is formed by three chiral ensembles [4] describing the spectrum of a massless Dirac operator near zero energy. The same symmetry is shared by tight-binding models with purely off-diagonal disorder at the band centre [5]. More recently, four more symmetry classes were identified [6], which characterize a dirty superconductor or a mesoscopic superconductor–normal metal system. The Hamiltonian matrix has in this case an additional block structure in the particle–hole space induced by the form of mean-field Bogoliubov–de Gennes equations for a superconductor. It was argued [7] that the extended classification scheme including ten classes (three Wigner–Dyson, three chiral and four Bogoliubov–de Gennes) is complete.

The classification of random matrix ensembles can be equally well applied to disordered electronic systems. In particular, two-dimensional systems of non-standard classes are of large interest, in view of their relevance to high-T_c superconductors, which have an unconventional (d-wave) symmetry of the order parameter and therefore possess low-energy quasiparticle excitations. In this paper, we will consider a system of class C, which is the Bogoliubov–de Gennes class with broken time-reversal but preserved spin rotation invariance. The corresponding Hamiltonian satisfies the symmetry $H^* = -\sigma_y H \sigma_y$ (with σ_y the Pauli matrix in the particle–hole space) and has the block structure

$$H = \begin{pmatrix} h & \Delta \\ \Delta^* & -h^T \end{pmatrix} \tag{1}$$

where $h = h^\dagger$ and $\Delta = \Delta^T$.

Similarly to the conventional Wigner–Dyson unitary class, a two-dimensional system of class C undergoes a transition between the phases with different quantized values of the Hall conductivity [8–10]. More precisely, since the quasiparticle charge is not conserved in a superconductor, one is led to consider the spin conductivity determining the spin current as a response to the gradient of the Zeeman magnetic field. The quantization of the Hall component of the spin conductivity tensor was named the spin quantum Hall (SQH) effect. It was shown [9] that the SQH effect can be realized in superconductors with $d_{x^2-y^2} + id_{xy}$ pairing symmetry explored in recent literature [11].

While the SQH transition shares many common features with its normal counterpart, it is qualitatively different as concerns the behaviour of the density of states (DOS) at criticality: while the DOS is uncritical for the conventional quantum Hall (QH) transition, it vanishes at the SQH critical point. A network model describing the SQH transition was constructed in [8], and critical exponents for the scaling of the localization length were determined numerically. In [9], a mapping onto a supersymmetric spin chain was performed, providing an alternative method for the numerical study of the critical behaviour. Remarkably, some exact analytical results for this problem have been obtained by mapping onto the classical percolation [10, 12, 13]. Specifically, it was found that the DOS scales as $\rho(\epsilon) \sim \epsilon^{1/7}$, while the average product of the retarded and advanced Green functions $\Pi(\mathbf{r}, \mathbf{r}') = \langle G_R(\mathbf{r}, \mathbf{r}') G_A(\mathbf{r}', \mathbf{r}) \rangle$ (referred to as the diffuson propagator, or the diffuson) and the average two-point conductance $\langle g(\mathbf{r}, \mathbf{r}') \rangle$ at $\epsilon = 0$ fall off as $|\mathbf{r} - \mathbf{r}'|^{-1/2}$.

It is known that critical wavefunctions at the conventional QH transition have multifractal nature [14, 15]. Recently, there has been a growth of activity in the direction of quantitative characterization of the corresponding spectrum of fractal dimensions [16–20]. Zirnbauer [17] and Bhaseen *et al* [18] proposed a certain supersymmetric σ-model with a Wess–Zumino–Novikov–Witten term (in two slightly different versions) as a candidate for the conformal field theory of the QH critical point. The theory implies an exactly parabolic form of

the multifractality spectrum. This was confirmed by a thorough numerical study of the wavefunction statistics at the QH transition [20].

The aim of this paper is to study the wavefunction statistics at the SQH critical point. We will demonstrate that the exponents Δ_2 and Δ_3 governing the scaling of the second and third moments of the wavefunction intensity (see section 2 for the formal definition) can be calculated exactly by analytical means. Quite surprisingly, we find that the index $\eta = -\Delta_2$ characterizing the spatial decay of the wavefunction correlations is equal to $1/4$, in contrast to the $r^{-1/2}$ decay of the diffusion propagator. This leads us to a general analysis of relations between different critical exponents characterizing the wavefunction statistics in the qualitatively new situation of the localization transition with a critical DOS. We complement our analytical results by numerical simulations, which allow us, in particular, to investigate whether the multifractality spectrum of the SQH critical point is exactly parabolic or not. The answer to this question, as well as the exact values of Δ_2 and Δ_3 we have found, is of central importance for identification of conformal theory of the SQH transition, which is the issue of considerable research interest at present [21–23]. Some of our results were reported in a brief form in [24].

The paper is organized as follows. In section 2 we remind the reader of some basic concepts related to the multifractality of critical wavefunctions. In section 3 we describe the network model of class C and use it to calculate numerically the DOS at the critical point of the SQH transition. In section 4 we present an analytical calculation which involves a mapping onto the percolation theory and allows us to calculate the averages of products of two and three Green functions and thus the exponents Δ_2 and Δ_3. Section 5 is devoted to a numerical evaluation of the full multifractal spectrum Δ_q. This allows us not only to check the analytical results of section 4 but also to investigate whether the spectrum is exactly parabolic (as for the conventional QH critical point) or not. In section 6 we present a numerical study of statistical properties of the two-point conductance. We further include a scaling analysis of the relation between the multifractal spectra of the two-point conductance and of the wavefunctions at a critical point with a vanishing DOS. These analytical arguments clarify the connection between the numerical findings of section 6 and the results of sections 4, 5 on the wavefunction multifractality. Finally, section 7 contains a summary of our results and a brief discussion of some remaining open problems.

2. Wavefunction multifractality in systems with non-critical DOS

Multifractality of wavefunctions $\psi(\mathbf{r})$ is known to be a hallmark of the localization transition. It has been extensively studied in the context of conventional Anderson and quantum Hall (QH) transitions with *non-critical* DOS (see [14, 15, 25], and references therein), and we remind the reader of some basic results. Multifractality is characterized by a set of exponents

$$\tau_q \equiv d(q-1) + \Delta_q \tag{2}$$

(d is the spatial dimensionality) describing the scaling of the moments of $|\psi^2(\mathbf{r})|$ with the system size L,

$$\langle |\psi(\mathbf{r})|^{2q} \rangle \sim L^{-d-\tau_q}. \tag{3}$$

Anomalous dimensions Δ_q distinguish a critical point from the metallic phase and determine the scale dependence of wavefunction correlations. Among them, $\Delta_2 \equiv -\eta$ plays the most prominent role, governing the spatial correlations of the 'intensity' $|\psi|^2$,

$$L^{2d} \langle |\psi^2(\mathbf{r})\psi^2(\mathbf{r}')| \rangle \sim (|\mathbf{r} - \mathbf{r}'|/L)^{-\eta}. \tag{4}$$

Equation (4) can be obtained from (3) by using the fact that the wavefunction amplitudes become essentially uncorrelated at $|\mathbf{r} - \mathbf{r}'| \sim L$. Scaling behaviour of higher-order spatial correlations, $\langle |\psi^{2q_1}(\mathbf{r_1})\psi^{2q_2}(\mathbf{r_2}) \ldots \psi^{2q_n}(\mathbf{r_n})| \rangle$ can be found in a similar way. Correlations of two different (but close in energy) eigenfunctions and the diffusion propagator $\Pi(\mathbf{r}, \mathbf{r}'; \omega) = \langle G_{E+\omega}^R(\mathbf{r}, \mathbf{r}') G_E^A(\mathbf{r}', \mathbf{r}) \rangle$ ($G^{R,A}$ are retarded and advanced Green functions) possess the same scaling properties,

$$\left. \begin{array}{l} L^{2d} \langle |\psi_i^2(\mathbf{r})\psi_j^2(\mathbf{r}')| \rangle \\ L^{2d} \langle \psi_i(\mathbf{r})\psi_j^*(\mathbf{r})\psi_i^*(\mathbf{r}')\psi_j(\mathbf{r}') \rangle \\ \rho^{-2}\Pi(\mathbf{r}, \mathbf{r}'; \omega) \end{array} \right\} \sim \left(\frac{|\mathbf{r} - \mathbf{r}'|}{L_\omega} \right)^{-\eta} \tag{5}$$

where $\omega = \epsilon_i - \epsilon_j$, $L_\omega \sim (\rho\omega)^{-1/d}$, ρ is the density of states and $|\mathbf{r} - \mathbf{r}'| < L_\omega$. In two dimensions the multifractal spectrum Δ_q plays a key role in the identification of the conformal field theory governing the critical point, which led to growing interest in the eigenfunction statistics at the QH transition [16–20].

Applying naively these results to the SQH transition, one would conclude that the $r^{-1/2}$ scaling of the diffusion propagator found in [10] implies $\eta = 1/2$. However, we show below that this conclusion is incorrect. This demonstrates that one should be cautious when trying to apply the relations between critical exponents obtained for systems with a non-critical DOS to those with a critical one (such as the SQH transition), as will be discussed in sections 4.3 and 6.

3. Network model and the density of states

As a model of the SQH system, we use the $SU(2)$ version [8] of the Chalker–Coddington network describing the QH transition [26]. Dynamics of the wavefunction defined on edges of the network is governed by a unitary evolution operator $\mathcal{U}$. At each node of the network the scattering from two incoming into two outgoing links is described by a matrix

$$S = \begin{pmatrix} \cos\theta & \sin\theta \\ -\sin\theta & \cos\theta \end{pmatrix} \tag{6}$$

with $\theta = \pi/4$ corresponding to the critical point. Each realization of the network is characterized by a set of random 2×2 spin matrices U_e associated with all edges e of the network. In view of (1), $\mathcal{U}$ satisfies the symmetry $\mathcal{U} = \sigma_y \mathcal{U}^* \sigma_y$, implying that $U_e \in SU(2)$. Diagonalizing $\mathcal{U}$ for a square network of size $L \times L$ yields $4L^2$ eigenfunctions $\psi_{i\alpha}(e)$ and eigenvalues $e^{-i\epsilon_i}$, where $i = 1, 2, \ldots, 4L^2$ and $\alpha = 1, 2$ is the spin index.

We begin by displaying in figure 1 the numerically calculated DOS $\rho(\epsilon)$ for different system sizes L. It is seen that after a proper rescaling all data collapse onto a single curve. Specifically, the energy axis is rescaled to ϵ/δ, where $\delta \propto L^{-7/4}$ is the level spacing at $\epsilon = 0$. (This scaling of δ is related to the critical behaviour of DOS $\rho(\epsilon) \sim \epsilon^{1/7}$ discussed below via the condition $\rho(\delta)\delta \sim 1/L^2$.) The scale invariance of $\rho(\epsilon)$ at criticality is reminiscent of the analogous property of the level statistics at the conventional Anderson or QH transition (see [25] for a review). At $\epsilon \gg \delta$ the critical DOS scales as $\rho(\epsilon) \sim \epsilon^{1/7}$, in agreement with analytical predictions [10]. On the other hand, at $\epsilon \sim \delta$ one observes an oscillatory structure qualitatively analogous to the behaviour found in the random matrix theory (RMT) for the class C [6].

Let us note that, strictly speaking, deviations of DOS from the RMT at $\epsilon \sim \delta$ are not parametrically small. On the other hand, the numerically found DOS follows very closely the RMT curve for two oscillation periods. In other words, the energy scale below which the RMT works (the effective Thouless energy), while being parametrically of order δ, turns out to
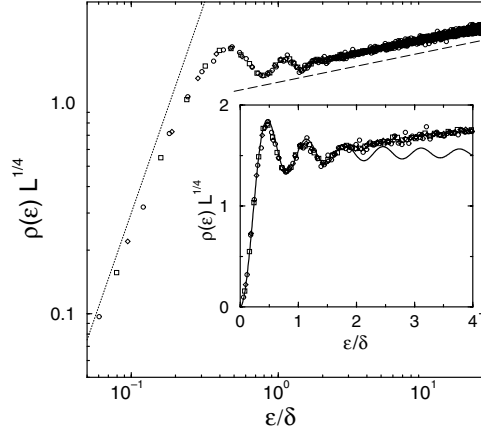
Figure 1. Scaling plot of the density of states for system sizes $L = 16$ ($\diamond$), 32 ($\square$), 96 ($\circ$). Dashed and dotted lines indicate power laws (dashed: $\epsilon^{1/7}$, dotted: ϵ^2), $\delta = 1/2\pi L^{7/4}$ denotes the level spacing at $\epsilon = 0$. Inset: same data on a linear scale and the result from the random matrix theory [6] (solid curve).

be several times larger. This indicates that there is a numerical smallness in the problem, and the SQH critical point shows 'close-to-metal' features (similar to the Anderson transition in $2 + \epsilon$ dimensions with small ϵ). The small value $1/7$ of the DOS exponent is another manifestation of the same fact.

The states with energies $\epsilon \gg \delta$ are localized with the localization length $\xi_\epsilon \sim \epsilon^{-4/7}$ [10]. For the smallest energies $\epsilon \sim \delta$ the correlation length ξ_ϵ is of the order of the system size. In view of their critical nature, these states are expected to be multifractal, $L^{2q} \langle |\psi_{i\alpha}(e)|^{2q} \rangle \sim L^{-\Delta_q}$. For $\epsilon \gg \delta$ the multifractality holds within a region of the extent ξ_ϵ (outside which the wavefunction is exponentially small); hence

$$L^2 \langle |\psi_{i\alpha}(e)|^{2q} \rangle \sim \xi_\epsilon^{-2(q-1)-\Delta_q} \equiv \xi_\epsilon^{-\tau_q}. \tag{7}$$

By the same token, spatial correlations are expected to be governed by the multifractality on scales below ξ_ϵ. In particular, we have for correlations of two different eigenfunctions with energies $\epsilon_i, \epsilon_j \sim \epsilon$

$$L^4 \langle |\psi_{i\alpha}(e)\psi_{j\beta}(e')|^2 \rangle \sim (r/\xi_\epsilon)^{\Delta_2} \qquad r \lesssim \xi_\epsilon \tag{8}$$

(r is the distance between e and e'), and similarly for higher-order correlators. In sections 4 and 5 we will demonstrate the multifractality explicitly and calculate the exponents Δ_q.

4. Two- and three-point correlation functions: mapping onto percolation problem

In this section, we present an analytical calculation of two- and three-point correlation functions, which allows us to find the fractal dimensions Δ_2 and Δ_3. We use the mapping onto the classical percolation, following the approach of [13], and demonstrate that it can be extended on products of two and three Green functions.

4.1. Two-point functions

Consider a correlation function of two wavefunctions,

$$\mathcal{D}(e', e; \epsilon_1, \epsilon_2) = \left\langle \sum_{ij\alpha\beta} \psi_{i\alpha}^*(e)\psi_{j\alpha}(e)\psi_{i\beta}(e')\psi_{j\beta}^*(e')\delta(\epsilon_1 - \epsilon_i)\delta(\epsilon_2 - \epsilon_j) \right\rangle \tag{9}$$

where e, e' are two different edges of the network. Introducing the Green function

$$G(e', e; z) = \langle e'|(1 - z\mathcal{U})^{-1}|e\rangle$$

(which is a 2×2 matrix in the spin space), we express (9) as

$$
\begin{aligned}
\mathcal{D}(e', e; \epsilon_1, \epsilon_2) = (2\pi)^{-2} \langle \text{Tr}[G_R(e', e; \text{e}^{\text{i}\epsilon_1}) - G_A(e', e; \text{e}^{\text{i}\epsilon_1})] \\
\times [G_R(e, e'; \text{e}^{\text{i}\epsilon_2}) - G_A(e, e'; \text{e}^{\text{i}\epsilon_2})]\rangle
\end{aligned}
\tag{10}
$$

where $G_{R,A}$ are retarded and advanced Green functions, $G_{R,A}(e', e; \text{e}^{\text{i}\epsilon_1}) = G(e', e; \text{e}^{\text{i}(\epsilon_1 \pm \text{i}0)})$. We will calculate (10) at zero energy, $\epsilon_{1,2} \to 0$, but finite level broadening, $\pm \text{i}0 \to \pm \text{i}\gamma$ with $\gamma \ll 1$. The scaling behaviour of the correlation function (9) at $\epsilon_1, \epsilon_2 \sim \epsilon$ can then be obtained by substituting ϵ for γ. We thus need to calculate

$$\mathcal{D}(e', e; \gamma) = (2\pi)^{-2} \langle \text{Tr}[G(e', e; z) - G(e', e; z^{-1})][G(e, e'; z) - G(e, e'; z^{-1})]\rangle \tag{11}$$

with a real $z = \text{e}^{-\gamma} < 1$. By the same token, in order to understand the scaling properties of another correlator of two wavefunctions,

$$\tilde{\mathcal{D}}(e', e; \epsilon_1, \epsilon_2) = \left\langle \sum_{ij\alpha\beta} |\psi_{i\alpha}(e)|^2 |\psi_{j\beta}(e')|^2 \delta(\epsilon_1 - \epsilon_i)\delta(\epsilon_2 - \epsilon_j) \right\rangle \tag{12}$$

we will consider the correlation function

$$\tilde{D}(e', e; \gamma) = (2\pi)^{-2} \langle \text{Tr}[G(e, e; z) - G(e, e; z^{-1})] \, \text{Tr}[G(e', e'; z) - G(e', e'; z^{-1})]\rangle. \tag{13}$$

As discussed at the end of section 3, the scaling behaviour of (11) and (13) at $r \ll \xi_\gamma$ (where r is the distance between e and e') is governed by the multifractal properties of wavefunctions (specifically, by the exponent Δ_2). The general strategy of calculation of the correlation functions (11), (13) is analogous to that used in [13] for the one-point function $\text{Tr}G(e, e; z)$. Therefore, we outline only briefly those steps which generalize directly the calculation in [13], and concentrate on qualitatively new aspects.

The Green functions in (11), (13) are straightforwardly represented in the form of a sum over paths

$$G(e, e'; z) = \sum_{\text{paths } e' \to e} \ldots \cdot z U_{e_j} s_j \cdot z U_{e_{j+1}} s_{j+1} \cdot \ldots \tag{14}$$

where s_j is the corresponding matrix element ($\cos\theta$, $\sin\theta$, or $-\sin\theta$) of the S-matrix between the edges e_j and e_{j+1}. Equation (14) generates a convergent expansion in powers of z when $|z| < 1$; otherwise, the identity

$$G^\dagger(e, e'; z) = \mathbf{1} \cdot \delta_{ee'} - G(e', e; (z^*)^{-1}) \tag{15}$$

is to be used (in all our calculations z is real, so that $z^* = z$). As shown below, each of the double sums over paths obtained by substituting (14), (15) in (11) or (13) can be reduced to a single sum over classical paths (hulls) in the percolation problem. This remarkable reduction crucially relies on the following two statements:

1. Only paths visiting each edge of the network either 0 or 2 times are to be taken into account; contributions of all the remaining paths sum up to zero,
2. Using statement 1, it is easy to see that each node may be visited 0, 2, or 4 times. The second statement concerns the nodes visited four times. As illustrated in figure 2, there are three possibilities how this may happen; the corresponding contributions have weights (i) $\cos^4\theta$, (ii) $\sin^4\theta$ and (iii) $-\sin^2\theta\cos^2\theta$ from the scattering matrix at this node. The statement is that one can equivalently take into account only the contributions (i) and (ii) with the weights $\cos^2\theta$ and $\sin^2\theta$, respectively.
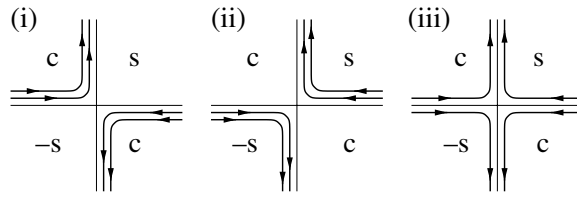
Figure 2. Possible configurations of paths passing four times through a network node. The symbols c and $\pm s$ denote the elements $\cos\theta$, $\pm\sin\theta$ of the S-matrix at the node.

In [13], both statements were proved for the case of the average of a single Green function $\langle G(e, e; z)\rangle$. We show below that they are valid for all the two-point functions entering (11), (13), as well as for averaged products of three Green functions (considered in section 4.2). Let us emphasize that such a generalization is far from trivial. This point is well illustrated by the fact that products of four (or more) Green functions determining the exponents Δ_q with $q = 4, 5, \ldots$ can *not* be mapped onto the percolation within our approach (see section 4.3 and the appendix).

We now proceed by proving statement 1. It is convenient for us to recall first the corresponding proof for the case of a single Green function, $\langle \text{Tr}\, G(e, e; z)\rangle$, considered in [13]. For an arbitrary edge f the paths entering (14) can be classified according to the number k of times they pass through f. The contribution of paths with $k \neq 0$ has the form

$$\sum_{k=1}^{\infty} \langle \text{Tr}\, B[U_f A(f, f)]^k\rangle \tag{16}$$

where B is a sum over all paths going from f to e and then from e to f, and $A(f, f)$ denotes a sum over paths which begin and end on f and do not return to f in between. Since $A(f, f)$ is a linear combination of $SU(2)$ matrices with real coefficients, it can be represented as $A(f, f) = |A(f, f)|\tilde{A}(f, f)$, where $\tilde{A}(f, f) \in SU(2)$ and $|A(f, f)|$ is a real number. After a change of the integration variable, $U_f \tilde{A}(f, f) \to U_f$, equation (16) then reduces to

$$\sum_{k=1}^{\infty} \langle \text{Tr}\, B U_f^k\rangle |A(f, f)|^k. \tag{17}$$

Since $SU(2)$ matrices can be represented as $U = \exp(i\alpha\mathbf{n}\boldsymbol{\sigma})$, with a real α and a unit vector $\mathbf{n}$ (σ_i are the Pauli matrices), one finds

$$U^k = \cos k\alpha \cdot \mathbf{1} + i \sin k\alpha\, \mathbf{n}\boldsymbol{\sigma}. \tag{18}$$

The $SU(2)$ invariant measure is $(2/\pi)\int_0^{\pi} d\alpha \sin^2\alpha \int d\mathbf{n}$, where $d\mathbf{n}$ is the conventional measure on the sphere. Therefore, for an integer k

$$\langle U^k\rangle = c_k \cdot \mathbf{1} \qquad c_k = \begin{cases} 1 & k = 0 \\ -\frac{1}{2} & k = 2, -2 \\ 0 & \text{otherwise.} \end{cases} \tag{19}$$

Substituting (19) in (17), one finds that only the term with $k = 2$ survives, which completes the proof of the statement 1 for the case of an average of one Green function.

We now turn to the products of two Green functions. Consider

$$\langle \text{Tr}\, G(e, e'; z)G(e'', e'''; z)\rangle \tag{20}$$

(we will need below both cases $e'' = e'$, $e''' = e$, and $e'' = e$, $e''' = e'$). Using (14), we classify the contributions to (20) according to the numbers of returns k_1, k_2 to the edge f for

the corresponding two paths. We want to show that only the contributions with $k_1 + k_2 = 0, 2$ are to be taken into account. If one of k_i is zero, the proof is obtained in the same way as for a single Green function (see above). We thus consider the remaining contributions, which are of the following form:

$$\sum_{k_1, k_2 = 1}^{\infty} \langle \mathrm{Tr}\, B_1 [U_f A(f, f)]^{k_1} B_2 [U_f A(f, f)]^{k_2} \rangle \tag{21}$$

where B_1 is a sum over the paths $f \to e$ and $e''' \to f$, and B_2 is a sum over the paths $f \to e''$ and $e' \to f$. Performing the variable change $U_f \tilde{A}(f, f) \to U_f$ as before, we get

$$\sum_{k_1, k_2 = 1}^{\infty} \langle \mathrm{Tr}\, B_1 U_f^{k_1} B_2 U_f^{k_2} \rangle |A(f, f)|^{k_1 + k_2}. \tag{22}$$

Using (18), we now calculate the average over U_f in (22):

$$\langle \mathrm{Tr}\, B_1 U_f^{k_1} B_2 U_f^{k_2} \rangle = \mathrm{Tr}\, B_1 B_2 \langle \cos k_1 \alpha \cos k_2 \alpha \rangle_\alpha - \frac{1}{3} \mathrm{Tr} \sum_i B_1 \sigma_i B_2 \sigma_i \langle \sin k_1 \alpha \sin k_2 \alpha \rangle_\alpha$$

$$= \frac{1}{2} \mathrm{Tr} \left(B_1 B_2 + \frac{1}{3} \sum_i B_1 \sigma_i B_2 \sigma_i \right) c_{k_1 + k_2} + \frac{1}{2} \mathrm{Tr} \left(B_1 B_2 - \frac{1}{3} \sum_i B_1 \sigma_i B_2 \sigma_i \right) c_{k_1 - k_2}$$

$$\equiv b_1 c_{k_1 + k_2} + b_2 c_{k_1 - k_2}. \tag{23}$$

The only property of the factors b_1, b_2 which is important for us at this stage is that they are independent of k_1, k_2. The sum (22) is therefore reduced to the form

$$\sum_{k_1, k_2 = 1}^{\infty} (b_1 c_{k_1 + k_2} + b_2 c_{k_1 - k_2}) |A(f, f)|^{k_1 + k_2}. \tag{24}$$

While the first term in brackets is non-zero only for $k_1 + k_2 = 2$ (i.e. $k_1 = k_2 = 1$) as required, the second one seems to spoil the proof. Let us perform, however, a summation over k_1 at fixed $k_1 + k_2 = k$. Using equation (19), we then find that the coefficients in the second term cancel for any even $k \geqslant 4$ (for odd k all terms are trivially zero):

$$\sum_{k_1 + k_2 = k} c_{k_1 - k_2} = c_{k-2} + c_{k-4} + \cdots + c_{-(k-2)}$$

$$= c_2 + c_0 + c_{-2} = 0. \tag{25}$$

Therefore, only the term with $k_1 = k_2 = 1$ survives in the sum (24), which completes the proof.[4]

Applying now the statement 2, the proof of which is given in the appendix, we represent each node as a superposition of contributions of types (i) and (ii) (figure 2) with weights $\cos^2 \theta$ and $\sin^2 \theta$, equal to $1/2$ at the SQH critical point. The network is then reduced to a weighted sum over all its possible decompositions in a set of closed loops (such that each edge belongs to exactly one loop). These loops can be viewed [10, 13] as hulls of the bond percolation problem. Non-zero contributions to the correlation function (20) come from pairs of paths retracing exactly twice a loop or a part of it. This yields for $z < 1$

$$\langle \mathrm{Tr}\, G(e', e; z) G(e, e'; z) \rangle = \langle \mathrm{Tr}\, G(e', e; z^{-1}) G(e, e'; z^{-1}) \rangle$$

$$= -2 \sum_N P(e', e; N) z^{2N} \tag{26}$$

---

[4] The correlation function $\langle \mathrm{Tr}\, G(e, e; z) \mathrm{Tr}\, G(e', e'; z) \rangle$ is analysed in the same way, yielding again a sum of type (24) so that our argument remains valid.

$$\langle \operatorname{Tr} G^2(e', e; z) \rangle = \langle \operatorname{Tr} G^2(e, e'; z^{-1}) \rangle$$
$$= -\sum_N P_1(e', e; N) z^{2N} \tag{27}$$

where $P(e', e; N)$ and $P_1(e', e; N)$ are probabilities that the edges e and e' belong to the same loop of the length N (resp. with the length N of the part corresponding to the motion from e to e'). Furthermore, to calculate the correlation function $\langle \operatorname{Tr} G(e', e; z) G(e, e'; z^{-1}) \rangle$ entering (11), we apply identity (15) to the second Green function and then use the property

$$\langle \operatorname{Tr} G(e', e; z) G^\dagger(e', e; z) \rangle = -2 \langle \operatorname{Tr} G^2(e', e; z) \rangle \tag{28}$$

following from the $SU(2)$ symmetry. As a result, we find

$$\langle \operatorname{Tr} G(e', e; z) G(e, e'; z^{-1}) \rangle = -2 \sum_N P_1(e', e; N) z^{2N} \tag{29}$$

and, combining (26) and (29),

$$\pi^2 D(e', e; \gamma) = \frac{1}{2} \sum_N [P_1(e', e; N) + P_1(e, e'; N)] z^{2N} - \sum_N P(e', e; N) z^{2N}. \tag{30}$$

Equations (26), (29), (30) express the quantum correlation functions entering (11) in terms of purely classical quantities $P(e', e; N)$ and $P_1(e', e; N)$. To analyse the results, we recall some facts from the percolation theory. It is known that the fractal dimension of the percolation hulls is 7/4 [27], implying (see [28] for a recent discussion) that P and P_1 scale as

$$P(e', e, N), \; P_1(e', e, N) \sim N^{-8/7} r^{-1/4} \qquad r \lesssim N^{4/7} \tag{31}$$

and fall off exponentially fast at $r \gg N^{4/7}$, where r is the distance between e and e'. This yields for the correlation functions in (26) and (29) (which we abbreviate as $\langle G_R G_R \rangle$, $\langle G_A G_A \rangle$, $\langle G_R G_A \rangle$)

$$\langle G_R G_R \rangle = \langle G_A G_A \rangle \simeq \langle G_R G_A \rangle \sim r^{-1/2} \qquad r \ll \xi_\gamma \equiv \gamma^{-4/7} \tag{32}$$

in full agreement with the scaling argument of [10]. However, these leading order terms cancel in (30) since

$$\sum_N P(e', e, N) = \sum_N P_1(e', e, N) = P(e', e) \tag{33}$$

where $P(e', e)$ is the probability that the edges e and e' belong to the same loop. The result is non-zero due to the factors z^{2N} only, implying that relevant N are now $N \sim \gamma^{-1}$, so that $\langle (G_R - G_A)(G_R - G_A) \rangle$ scales differently compared to (32),

$$\mathcal{D}(e', e; \gamma) = \frac{1}{\pi^2} \sum_N [P(r, N) - P_1(r, N)](1 - e^{-2N\gamma})$$
$$\sim P(r, \gamma^{-1}) \gamma^{-1} \sim (\xi_\gamma r)^{-1/4} \qquad r \lesssim \xi_\gamma. \tag{34}$$

Using now definition (9) of $\mathcal{D}$ and the DOS scaling, $\rho(\epsilon) \sim \epsilon^{1/7} \sim \xi_\epsilon^{-1/4}$, we find for $r \lesssim \xi_\epsilon$

$$L^4 \langle \psi_{i\alpha}^*(e) \psi_{j\alpha}(e) \psi_{i\beta}(e') \psi_{j\beta}^*(e') \rangle \sim (r/\xi_\epsilon)^{-1/4}. \tag{35}$$

The correlation function (13) is calculated in a similar way. The results for the $\langle G_R G_R \rangle$, $\langle G_A G_A \rangle$ and $\langle G_R G_A \rangle$ terms in (13) have the form

$$\langle \operatorname{Tr} G(e, e; z) \operatorname{Tr} G(e', e'; z) \rangle = 4 - 2 \sum_N [P(e; N) + P(e'; N)] z^{2N}$$
$$+ \sum_{NN'} P_-(e, e'; N, N') z^{2(N+N')} + \sum_N P(e, e'; N) z^{2N} \tag{36}$$

$$\langle \operatorname{Tr} G(e, e; z^{-1}) \operatorname{Tr} G(e', e'; z^{-1}) \rangle = \sum_{NN'} P_-(e, e'; N, N') z^{2(N+N')} + \sum_N P(e, e'; N) z^{2N} \quad (37)$$

$$\langle \operatorname{Tr} G(e, e; z) \operatorname{Tr} G(e', e'; z^{-1}) \rangle = 2 \sum_N P(e'; N) z^{2N} - \sum_{NN'} P_-(e, e'; N, N') z^{2(N+N')}$$

$$- \sum_N P(e, e'; N) z^{2N} \quad (38)$$

where $P(e; N)$ is the probability that e belongs to a loop of length N, while $P_-(e, e'; N, N')$ is the probability that e and e' belong to different loops of lengths N and N', respectively. A larger number of terms in (36)–(38) as compared to (26), (29) is because of two reasons. First, there is a unit matrix contribution of a 'path of zero length' to the expansion (14) of the Green function $G(e, e; z)$. Second, e and e' may now belong to different loops and still give a finite contribution, since each of the two paths will retrace twice the corresponding loop.

Combining (36)–(38) and using the identities

$$P(e, e'; N) + \sum_{N'} P_-(e, e; N, N') = P(e; N) \quad (39)$$

$$\sum_N P(e; N) = 1 \quad (40)$$

we get for the correlation function (13)

$$\pi^2 \tilde{\mathcal{D}}(e', e; \gamma) = \sum_N P(e, e'; N)(1 - z^{2N}) + \sum_{NN'} P_-(e, e'; N, N')(1 - z^{2N})(1 - z^{2N'}). \quad (41)$$

We see again that at $z \equiv e^\gamma = 1$ the result is zero, and that at small γ it is dominated by $N \sim \gamma^{-1}$. Using equation (31) and

$$P_-(e, e'; N, N') \sim P(e; N) P(e'; N') \sim N^{-8/7} (N')^{-8/7} \quad (42)$$

we find that the first term in (41) is $\sim \xi_\gamma^{-1/4} r^{-1/4}$ at $r \ll \xi_\gamma$, while the second one is $\sim \xi_\gamma^{-1/2}$ and thus can be neglected. Therefore, we find that $\tilde{\mathcal{D}}$ shows the same scaling behaviour as $\mathcal{D}$ (see equation (34)),

$$\tilde{\mathcal{D}}(e', e; \gamma) \simeq \sum_N P(e, e'; N)(1 - e^{-2N\gamma}) \sim \xi_\gamma^{-1/4} r^{-1/4} \qquad r \ll \xi_\gamma. \quad (43)$$

In other words, the wavefunction correlator $\langle |\psi_{i\alpha}^2(e) \psi_{j\beta}^2(e')| \rangle$ with $\epsilon_i, \epsilon_j \sim \epsilon$ scales at $r \lesssim \xi_\epsilon$ in the same way as (35),

$$L^4 \langle |\psi_{i\alpha}^2(e) \psi_{j\beta}^2(e')| \rangle \sim \rho^{-2}(\epsilon) \tilde{\mathcal{D}}(e', e; \gamma \sim \epsilon) \sim (r/\xi_\epsilon)^{-1/4}. \quad (44)$$

Both equations (35) and (44) imply that the fractal exponent

$$\eta \equiv -\Delta_2 = \tfrac{1}{4} \quad (45)$$

at variance with what one might naively expect from the $r^{-1/2}$ scaling of the diffusion propagator $\langle G_R G_A \rangle$, equation (32).

4.2. Three-point functions

We now consider averaged products of three Green functions, analogous to the two-point functions (11) and (13),

$$\mathcal{D}(e, e', e''; \gamma) = (2\pi)^{-3} \langle \operatorname{Tr} [G(e, e'; z) - G(e, e'; z^{-1})][G(e', e''; z) - G(e', e''; z^{-1})]$$

$$\times [G(e'', e; z) - G(e'', e; z^{-1})] \rangle \quad (46)$$

$$\tilde{D}(e, e', e''; \gamma) = (2\pi)^{-3} \langle \text{Tr}\, [G(e, e; z) - G(e, e; z^{-1})] \text{Tr}\, [G(e', e'; z) - G(e', e'; z^{-1})]$$
$$\times \text{Tr}\, [G(e'', e''; z) - G(e'', e''; z^{-1})] \rangle. \tag{47}$$

The key role in the calculation of (46) and (47) is played by the proofs of applicability of statements 1 and 2 (section 4.1) to the products of three Green functions. Details of these proofs are given in the appendix. After the two statements are applied and the network is reduced to a sum over its loop decompositions (as in section 4.1), the correlation functions are calculated straightforwardly. In particular, we find for the averaged products of three Green functions entering (46)

$$\langle \text{Tr}\, G(e, e'; z) G(e', e''; z) G(e'', e; z) \rangle = - \sum_N [3P(e, e', e''; N) + P(e'', e', e; N)] z^{2N} \tag{48}$$

$$\langle \text{Tr}\, G(e, e'; z^{-1}) G(e', e''; z^{-1}) G(e'', e; z^{-1}) \rangle = \sum_N [P(e, e', e''; N) + 3P(e'', e', e; N)] z^{2N} \tag{49}$$

$$\langle \text{Tr}\, G(e, e'; z) G(e', e''; z) G(e'', e; z^{-1}) \rangle = -2 \sum_N P_1(e, e', e''; N) z^{2N} \tag{50}$$

$$\langle \text{Tr}\, G(e, e'; z^{-1}) G(e', e''; z^{-1}) G(e'', e; z) \rangle = 2 \sum_N P_1(e'', e', e; N) z^{2N} \tag{51}$$

where $P(e, e', e''; N)$ is the probability that the edges e, e' and e'' belong to the same loop of length N, with e' lying on the path from e'' to e, while $P_1(e, e', e''; N)$ is the same probability but with N being the length of the segment from e'' to e. Combining equations (48)–(51), we express the correlation function (46) in terms of the classical probabilities P and P_1. Remarkably, the situation is qualitatively different as compared to the calculation of two-point functions (section 4.1): the leading terms in (48)–(51) do *not* cancel in the expression for $D(e, e', e''; \gamma)$. We can thus simply set $\gamma = 0$ ($z = 1$), which yields

$$(2\pi)^3 D(e, e', e''; \gamma) \simeq 2[P(e, e', e'') + P(e'', e', e)] \qquad r \ll \xi_\gamma \tag{52}$$

where $P(e, e', e'') = \sum_N P(e, e', e''; N)$ is the probability for e, e' and e'' to belong to the same loop with the orientation $e \leftarrow e' \leftarrow e'' \leftarrow e$, and r is the characteristic scale of the distances between e, e' and e''.

The correlation function (47) is calculated in the same way, and the results are qualitatively similar. We thus skip intermediate formulae and only present the final result

$$(2\pi)^3 \tilde{D}(e, e', e''; \gamma) \simeq 8[P(e, e', e'') + P(e'', e', e)] \qquad r \ll \xi_\gamma \tag{53}$$

which differs from (52) by an overall factor of 4 only.

Using either of equations (52), (53), we can determine the fractal exponent Δ_3. In analogy with (31), the probability for the edges e, e' and e'' separated by distances $\sim r$ to belong to the same loop (percolation hull) of a length N scales as

$$P(e, e', e''; N) \sim N^{-8/7} r^{-1/2} \qquad r \lesssim N^{4/7} \tag{54}$$

and is exponentially small for $r \gg N^{4/7}$. Summing over N, we thus get

$$P(e, e', e'') \sim r^{-3/4}. \tag{55}$$

Substituting this in equations (52), (53) and expressing D and $\tilde{D}$ in terms of wavefunctions in analogy with the two-point functions (9), (12), we find for $r \lesssim \xi_\epsilon$

$$L^6 \langle \psi_{i\alpha}(e) \psi_{i\beta}^*(e') \psi_{j\beta}(e') \psi_{j\gamma}^*(e'') \psi_{k\gamma}(e'') \psi_{k\alpha}^*(e) \rangle,$$

$$L^6 \langle |\psi_{i\alpha}(e) \psi_{j\beta}(e') \psi_{k\gamma}(e'')|^2 \rangle \sim \frac{r^{-3/4}}{\rho^3(\epsilon)} \sim (r/\xi_\epsilon)^{-3/4}. \tag{56}$$

Therefore, the exponent Δ_3 is equal to

$$\Delta_3 = -\tfrac{3}{4}. \tag{57}$$

4.3. Discussion

The situation we encountered while calculating two- and three-point functions is qualitatively different from what happens at conventional localization transitions. Specifically, in the conventional case average products of only retarded or only advanced Green functions are negligible compared to mixed averages containing both G_R and G_A, e.g. $\langle G_R G_R \rangle$, $\langle G_A G_A \rangle \ll \langle G_R G_A \rangle$. For this reason, the wavefunction correlators, which are proportional to $\langle (G_R - G_A)(G_R - G_A) \rangle$, are determined by $\langle G_R G_A \rangle$ (and similarly for higher moments). In contrast, we have found in the SQH case that the correlators of the $\langle G_R G_R \rangle$ (or $\langle G_A G_A \rangle$) type are approximately equal to $\langle G_R G_A \rangle$ and cancel it in the leading order (so that $\langle (G_R - G_A)(G_R - G_A) \rangle$ scales differently). Evaluation of three-point functions made the overall picture even more complex: while we obtained again an identical scaling of, say, $\langle G_R G_R G_R \rangle$ and $\langle G_R G_R G_A \rangle$ correlators, this time the cancellation was not complete, and the correlation function $\langle (G_R - G_A)(G_R - G_A)(G_R - G_A) \rangle$ scaled in the same way.

To shed more light on the reason for these different types of scaling behaviour, it is instructive to reverse the logic and examine how the diffuson scaling (32) can be obtained from wavefunction correlations (35). It is straightforward to express the zero-energy diffusion propagator in terms of the correlation function $\mathcal{D}(e', e; \epsilon_1, \epsilon_2)$ defined in equation (10),

$$\Pi(e', e) \equiv \langle \text{Tr}\, G_R(e', e; 1) G_A(e, e'; 1) \rangle = \int \frac{\mathrm{d}\epsilon_1\, \mathrm{d}\epsilon_2}{(1 - \mathrm{e}^{-\mathrm{i}\epsilon_1 + 0})(1 - \mathrm{e}^{-\mathrm{i}\epsilon_2 - 0})} \mathcal{D}(e', e; \epsilon_1, \epsilon_2). \tag{58}$$

As discussed in section 4.1, $\mathcal{D}(e', e; \epsilon_1, \epsilon_2)$ scales with the distance $r = |e' - e|$ and the energy $\epsilon_{1,2} \sim \epsilon$ as follows

$$\mathcal{D}(e', e; \epsilon_1, \epsilon_2) \sim (r/\xi_\epsilon)^{\Delta_2} \xi_\epsilon^{-2x_\rho} \qquad r \ll \xi_\epsilon \tag{59}$$

where $\Delta_2 = -1/4$, $x_\rho = 1/4$ is the scaling dimension of DOS defined by $\rho(\epsilon) \sim \xi_\epsilon^{-x_\rho}$, and $\xi_\epsilon = \epsilon^{-1/(2-x_\rho)} = \epsilon^{-4/7}$. (For $r \gg \xi_\epsilon$ the function $\mathcal{D}(e', e; \epsilon_1, \epsilon_2)$ is exponentially small.)

Substituting (59) in (58), we see that if $2x_\rho + \Delta_2 > 0$, which is the case for the SQH transition, the energy integral in (58) is dominated by $\epsilon_{1,2} \sim \epsilon(r)$, where $\epsilon(r)$ is defined by $\xi_{\epsilon(r)} \sim r$ (i.e. $\epsilon(r) \sim r^{-(2-x_\rho)} = r^{-7/4}$), and can be estimated as

$$\begin{aligned} \Pi(e', e) &\sim \mathcal{D}(e', e; \epsilon_1, \epsilon_2)|_{\epsilon_{1,2} \sim \epsilon(r)} \\ &\sim r^{-2x_\rho} = r^{-1/2} \end{aligned} \tag{60}$$

in full agreement with the exact result (32).[5] This is in stark contrast with the case of a conventional localization (Anderson or QH) transition, when the diffusion propagator Π (or any other correlation function of the $\langle G_R G_A \rangle$ type) depends in a singular way on the infrared cutoff set by L_ω, see the last line of equation (5). On the other hand, equation (60) has the familiar form of a two-point correlator in a conformal field theory (or, more generally, in a field-theoretical description of standard critical phenomena), where $\langle \mathcal{O}_i(\mathbf{r}_1) \mathcal{O}_i(\mathbf{r}_2) \rangle$ scales as $|\mathbf{r}_1 - \mathbf{r}_2|^{-2x_i}$, with x_i being the scaling dimension of the operator $\mathcal{O}_i$.

---

[5] Since integral (58) is determined by the upper cutoff $\epsilon(r)$ (and not by the vicinity of $\epsilon = 0$), this calculation applies not only to $\Pi = \langle G_R G_A \rangle$, but equally well to $\langle G_R G_R \rangle$ and $\langle G_A G_A \rangle$, in agreement with (32).

Generalization to higher moments is straightforward. We define a wavefunction correlation function

$$\mathcal{D}^{(q)}(e_1, \ldots, e_q; \epsilon_1, \ldots, \epsilon_q) = (2\pi)^{-q} \langle \mathrm{Tr}\, [(G_R - G_A)(e_1, e_2; \mathrm{e}^{\mathrm{i}\epsilon_1})(G_R - G_A)(e_2, e_3; \mathrm{e}^{\mathrm{i}\epsilon_2})$$
$$\times \cdots \times (G_R - G_A)(e_q, e_1; \mathrm{e}^{\mathrm{i}\epsilon_q})] \rangle \tag{61}$$

and a set of $\langle G \ldots G \rangle$ correlation functions,

$$\Pi^{(q)}_{s_1 \ldots s_q}(e_1, \ldots, e_q; \epsilon_1, \ldots, \epsilon_q) = \langle \mathrm{Tr}\, G_{s_1}(e_1, e_2; \mathrm{e}^{\mathrm{i}\epsilon_1}) \ldots G_{s_q}(e_q, e_1; \mathrm{e}^{\mathrm{i}\epsilon_q}) \rangle \tag{62}$$

where $s_j = R$ or A. Assuming that all distances between the points e_i are $\sim r$, we have in analogy with (59),

$$\mathcal{D}^{(q)}(e_1, \ldots, e_q; \epsilon_1, \ldots, \epsilon_q) \sim (r/\xi_\epsilon)^{\Delta_q} \xi_\epsilon^{-q x_\rho} \qquad r \lesssim \xi_\epsilon. \tag{63}$$

Writing for $\Pi^{(q)}_{s_1 \ldots s_q}$ a spectral representation of type (58), we see that the integrals are determined by the upper limit $\epsilon \sim \epsilon(r) = r^{-(2-x_\rho)}$ provided

$$\Gamma(q) \equiv q x_\rho + \Delta_q > 0. \tag{64}$$

Under this condition, we find that $\Pi^{(q)}_{s_1 \ldots s_q}$ is in fact independent of the indices s_i and scales as

$$\Pi^{(q)}_{s_1 \ldots s_q}(e_1, \ldots, e_q; \epsilon_1, \ldots, \epsilon_q) \sim r^{-q x_\rho}. \tag{65}$$

For larger q, when $q x_\rho + \Delta_q < 0$, the energy integrals are dominated by the vicinity of $\epsilon = 0$. Consequently, the correlation functions $\Pi^{(q)}_{s_1, \ldots, s_q}$ start to depend in a singular way on the infrared cutoff (ξ_ϵ) and are expected to scale in the same way as $\mathcal{D}^{(q)}$, equation (63) (with a numerical prefactor depending on indices s_i), similar to the conventional Anderson localization transition.

The value of q separating the two regimes is thus determined by the equation $q x_\rho + \Delta_q = 0$. For the SQH transition ($x_\rho = 1/4$) its solution is, in view of equation (57), $q = 3$. Remarkably, this is also the largest value of q for which the mapping onto percolation described above still works (see the appendix). We believe that this is not a mere coincidence. Indeed, within this mapping average products $\Pi^{(q)}_{s_1 \ldots s_q}$ of Green functions are expressed in terms of probabilities of the percolation theory, and are therefore of order unity for $r \sim 1$. On the other hand, equation (63) yields, in the regime $q x_\rho + \Delta_q < 0$, a result which is much larger than unity at $r \sim 1, \xi_\epsilon \gg 1$ and diverges in the absence of the infrared cutoff, $\xi_\epsilon \to \infty$. We see no way such behaviour might be produced by the percolation theory.

Finally, we discuss a relation between our consideration and the field-theoretical approach to the wavefunction multifractality [18, 23, 29–32]. In the renormalization-group language, $\Gamma(q)$ defined by equation (64) are scaling dimensions of operators of the type $\mathcal{O}^{(q)} \sim \psi_{s_1} \psi^\dagger_{s'_1} \ldots \psi_{s_q} \psi^\dagger_{s'_q}$, where $\psi, \psi^\dagger$ are electronic fields. Averaged products of Green functions are expressed as correlation functions of the corresponding operators $\mathcal{O}^{(q)}$; in particular, (62) takes the form

$$\Pi^{(q)}_{s_1 \ldots s_q} \sim \langle \mathrm{Tr}\, \mathcal{O}^{(1)}_{s_1 s_2}(e_2) \mathcal{O}^{(1)}_{s_2 s_3}(e_3) \ldots \mathcal{O}^{(1)}_{s_q s_1}(e_1) \rangle. \tag{66}$$

To calculate the scaling behaviour of such correlation functions, one applies the operator product expansion (OPE) [30–32]. Generically, the identity operator will be among those generated by the OPE. Moreover, under the condition $\Gamma(q) > 0$ (equation (64)) it will be the most relevant operator and will dominate the expansion, leading to the gap scaling $\Pi^{(q)} \sim r^{-q\Gamma(1)}$, in agreement with (65). On the other hand, if $\Gamma(q) < 0$, the operator $\mathcal{O}^{(q)}$ will give a dominant contribution to OPE, leading to a multifractal type of scaling, $\Pi^{(q)} \propto r^{-q\Gamma(1)}(r/\xi_\epsilon)^{\Gamma(q)}$, as in equation (63). What is, however, non-trivial from this point of view, is that the scaling of the wavefunction correlator (61) has the multifractal form (63)

independent of the sign of $\Gamma(q)$. This means that in the regime $\Gamma(q) > 0$ the leading (gap scaling) terms (65) cancel in the particular combination of the functions $\Pi^{(q)}$ corresponding to $\mathcal{D}^{(q)}$, and subleading terms determine the result (63). A similar cancellation of leading scaling terms in the context of classical percolation was recently discussed in [28].

5. Wavefunction statistics: numerical results

5.1. Multifractality spectrum

The analytical treatment of section 4 yielded results for the anomalous dimensions at two distinct values of q, $\Delta_2 = -1/4$ and $\Delta_3 = -3/4$. In order to obtain more complete information about the wavefunction statistics, namely the multifractality spectrum at arbitrary q, we have performed numerical simulations. A question we are particularly interested in is whether or not the spectrum is exactly parabolic. A definite answer to this question will imply, along with exact values of Δ_2 and Δ_3, an important constraint on the conformal theory of the critical point, which is a subject of current research [21–23].

Before we come to the presentation of our findings, we give a few remarks about technical aspects of our numerics. We compute wavefunctions by numerically diagonalizing the $4L^2 \times 4L^2$ unitary time evolution operator $\mathcal{U}$ of the Chalker–Coddington network described in section 3. Using advanced sparse matrix packages [33], we selectively calculate only states with energies in the vicinity of $\epsilon = 0$, which are critical over the whole extent of the system ($\xi_\epsilon \sim L$). Specifically, we consider, for each realization of the network, four lowest eigenstates (i.e. with eigenvalues $e^{-i\epsilon}$ closest to unity). The number of wavefunctions in a statistical ensemble we obtain this way ranges from about 10^7 for $L = 16$ to 2×10^4 for $L = 384$.

To determine the multifractality spectrum τ_q, we calculate for each wavefunction ψ_i the generalized inverse participation ratio (IPR)

$$P_q = \sum_{\alpha e} |\psi_{i\alpha}(e)|^{2q} \tag{67}$$

and analyse the scaling of the average $\langle P_q \rangle$ with the system size L. The data can be fitted very well by the power law

$$\langle P_q \rangle = c_q (2L)^{-\tau_q}. \tag{68}$$

To demonstrate this, we show in figure 3 the system size dependence of $\langle P_q \rangle (2L)^{\tau_q}$, with τ_q obtained from the fit. The plot is organized in such a way that a pure power law (68) would correspond to a horizontal line. This kind of plot is very sensitive to any corrections to a pure power-law behaviour of $\langle P_q \rangle$. Since no systematic curvature is observed, corrections to scaling are extremely small. This allows us to determine the anomalous dimensions $\Delta_q = \tau_q + 2(1-q)$ with great accuracy.

The obtained results for Δ_q are shown by a solid line in the upper panel of figure 4. We choose to plot $\Delta_q/q(1-q)$, since this would give a constant for an exactly parabolic spectrum, which is uniquely determined by η, $\Delta_q = \eta q(1-q)/2$. According to our analytical calculations (section 4), $\Delta_q/q(1-q)$ is equal to $1/8$ for both $q = 2$ and $q = 3$; this value is marked by the dashed line in the figure. It is seen that the numerical results agree perfectly well with the analytical findings at $q = 2$ and $q = 3$. Furthermore, the parabolic dependence may serve as a numerically good approximation in the whole range of q we studied,

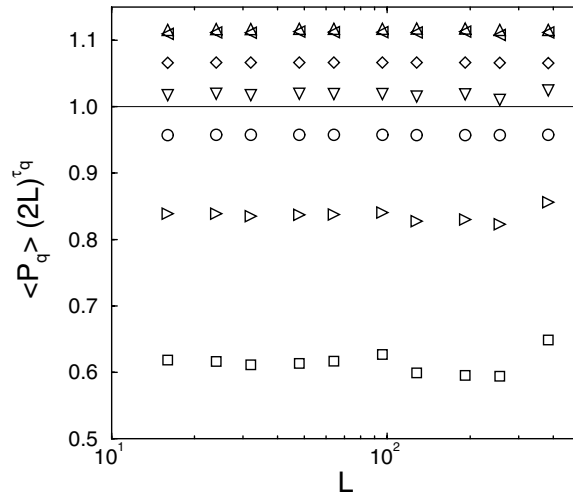$$\Delta_q \simeq \frac{q(1-q)}{8}. \tag{69}$$

Figure 3. Scaling of the average IPR with the system size L for several values of $q = 0.5$ ($\circ$), 1.5 ($\diamond$), 2 ($\triangle$), 2.5 ($\triangleleft$), 3 ($\triangledown$), 3.5 ($\triangleright$), 4 ($\square$). The system size dependence of the amplitude $c_q(L) \equiv \langle P_q \rangle (2L)^{\tau_q}$ is presented, with $\tau_q \equiv 2(q-1) + \Delta_q$ shown in figure 4. The scattering of the data is due to the limited size of the statistical ensemble used. The solid line is a guide to the eye corresponding to the vanishing of finite size corrections ($c_q(L) = \text{const}$).
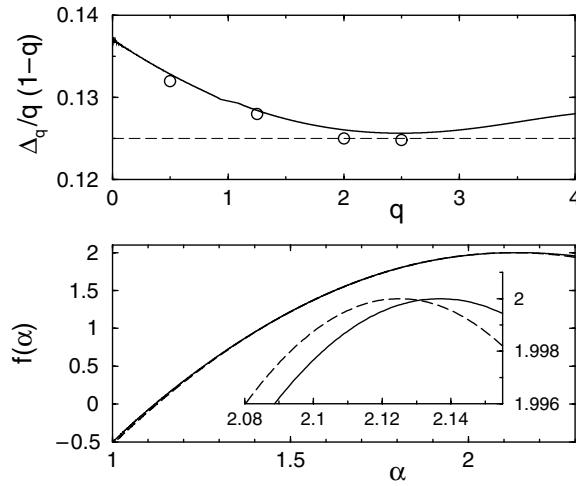

Figure 4. Upper panel: anomalous dimension Δ_q (solid line) describing the scaling of the average IPR $\langle P_q \rangle$. The functional form $\Delta_q/q(1-q)$ highlights the deviation from exact parabolicity (69) indicated by the dashed line. The circles correspond to the exponent $\tilde{\Delta}_q$ obtained from the scaling of the typical value P_q^{typ}. Lower panel: singularity spectrum $f(\alpha)$, numerical results (solid line) and the parabolic approximation (70) (dashed line) are shown. The inset depicts a magnification of the apex region; the deviations from (70) correspond to the enhancement of $\Delta_q/q(1-q)$ near $q = 0$ in the upper graph.

Nevertheless, we believe that equation (69) is not exact. Indeed, at $0 < q < 2$ the numerically found Δ_q show clear deviations from exact parabolicity (69), which are of the order of 10% near $q = 0$. Since this is precisely the regime in which finite-size effects have been found to be very weak and Δ_q was determined with a high accuracy, we interpret the observed deviations

as very strong evidence for nonparabolicity of the exact multifractal spectrum of the SQH transition. In particular, the deviation of the limiting value $\Delta_q/q(1-q)|_{q\to0} = 0.137 \pm 0.003$ from 1/8 well exceeds the estimated numerical uncertainty.

We also calculated typical inverse participation ratios, $P_q^{\text{typ}} = \exp\langle\ln P_q\rangle$ and the corresponding dimensions $\tilde{\tau}_q \equiv 2(q-1) + \tilde{\Delta}_q$.[6] It follows from the general analysis of the wavefunction multifractality [34] that $\tilde{\tau}_q = \tau_q$ for $q \leqslant q_c$, where q_c corresponds to the zero α_- of the singularity spectrum $f(\alpha)$ (defined below). In the present case we find from the Δ_q data $q_c = 3.9 \pm 0.1$ (the parabolic approximation (69) would imply $q_c = 4$). For $q > q_c$ the average $\langle P_q\rangle$ is determined by rare realizations, and $\tau_q < \tilde{\tau}_q$. Furthermore, already for q smaller than but close to q_c, finite-size corrections to P_q^{typ} become large [20], leading to large errors in the determination of $\tilde{\tau}_q$. For the SQH problem, we find that the scaling of P_q^{typ} exhibits small finite-size corrections as long as $q \leqslant 2.5$, so that the corresponding exponents $\tilde{\tau}_q$ can be found with a high accuracy. The results are shown by circles in figure 4 (upper panel) and are in full agreement with the values of τ_q obtained from the scaling of $\langle P_q\rangle$. For larger q ($q \geqslant 3$) the finite-size corrections to P_q^{typ} (which we estimate to be $\sim L^{-y}$ with $y \approx 0.4$) become appreciable, strongly reducing the accuracy of determination of $\tilde{\tau}_q$.

The lower panel of figure 4 depicts the singularity spectrum $f(\alpha)$ obtained by a numerical Legendre transform of the scaling dimension τ_q, $f(\alpha_q) = q\alpha_q - \tau_q$ with $\alpha_q = \mathrm{d}\tau_q/\mathrm{d}q$. The dashed line represents the parabolic approximation corresponding to (69),

$$f(\alpha) = 2 - \frac{(\alpha - \alpha_0)^2}{4(\alpha_0 - 2)} \qquad \alpha_0 - 2 = 1/8. \tag{70}$$

We see again that the parabolic approximation is numerically rather good; nevertheless, it is not exact. Deviations from (70) are demonstrated in the inset which shows an enlarged view of a region around the maximum α_0 of $f(\alpha)$. The deviation of $\alpha_0 - 2 = 0.137 \pm 0.003$ from 1/8 corresponds to the non-parabolicity of τ_q discussed above.

5.2. IPR fluctuations

We devote the remainder of this section to a brief discussion of the IPR distribution function $\mathcal{P}(P_q)$, specifically, its evolution with the system size L and dependence on q. In analogy with Anderson and quantum Hall transitions studied earlier [20, 34–37], we expect the distribution $\mathcal{P}(P_q)$ to become scale-invariant in the large-L limit. Figure 5 demonstrates that this is indeed the case. It represents the evolution of the distribution of $\ln P_2$ with the system size L. The mean of the distribution is shifted as $-\tilde{\tau}_2 \ln L$. Apart from small statistical fluctuations at the largest system sizes, a clear tendency towards an asymptotic form is observed. To characterize the width of the distribution $\mathcal{P}(\ln P_q)$, we calculate the variance $\sigma_q^2 = \text{var}(\ln P_q)$, as shown in the inset of figure 5 for $q = 2$. The results extrapolated to $L \to \infty$ (the finite-size corrections are again of the type L^{-y} with $y \approx 0.4$) are presented in figure 6. The behaviour of σ_q is qualitatively similar to that found for other localization transitions. A somewhat unusual feature of the SQH transition is that in a rather broad range $0 \leqslant q \leqslant 3$ the variance σ_q^2 is remarkably well described by the formula

$$\sigma_q^2 = \text{const} \times q^2(q-1)^2 \tag{71}$$

which has been derived for a metallic system [25, 38], or for the Anderson transition with a weak multifractality, e.g. in $2 + \epsilon$ dimensions [34, 36]. In the latter case this formula is valid for $q \ll q_c$. The accuracy of equation (71) is one more manifestation of the 'close-to-metal'

---

[6] In our earlier publications [20, 34, 36] we used the symbol τ_q to characterize the scaling of the typical value P_q^{typ}, and $\tilde{\tau}_q$ for the average $\langle P_q\rangle$. In the present paper we have chosen to interchange the notation.
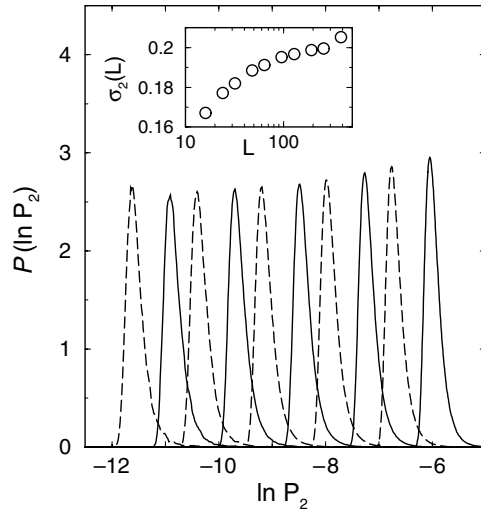
Figure 5. Distribution function $\mathcal{P}(\ln P_2)$ for system sizes $L = 16, 24, 32, 48, 64, 96, 128, 192, 256, 384$ (from right to left). For values of L large enough, the form of the distribution becomes independent of L. Inset: width $\sigma_2(L) = \langle(\ln P_2 - \langle\ln P_2\rangle)^2\rangle^{1/2}$ of the distribution $\mathcal{P}(\ln P_2)$ versus the system size L. Some scattering of the data for the largest system sizes is due to the limited number of samples.
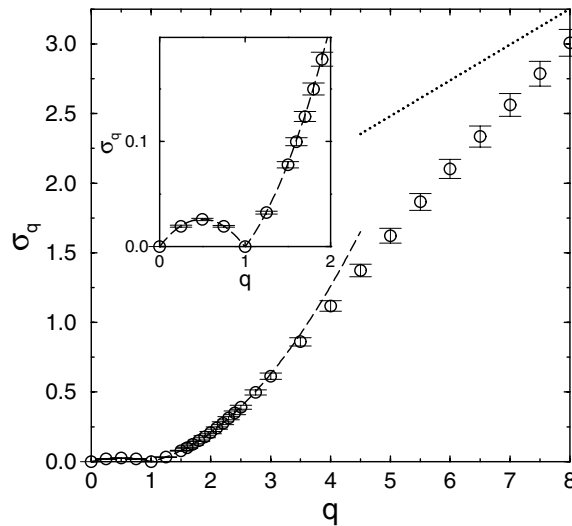

Figure 6. R.m.s. deviation $\sigma_q = \langle(\ln P_q - \langle\ln P_q\rangle)^2\rangle^{1/2}$ of the IPR logarithm. The dashed line is a fit to equation (71), the dotted line corresponds to the asymptotic limit $\sigma_q = q/q_c$ with $q_c = 3.9$. The inset shows an enlarged view of the low-q region.

character of the SQH critical point already mentioned in section 3, which leads to a relatively large value of $q_c \simeq 4$. At larger q, the behaviour of σ_q becomes linear (as was also found for the conventional Anderson transition [36, 37]), in agreement with the theoretical prediction $\sigma_q = q/q_c$ for $q \gg q_c$ [36]. This is because in this regime the distribution $\mathcal{P}(P_q)$ is dominated by a slowly decaying power-law tail $\mathcal{P}(P_q) \propto P_q^{-1-x_q}$, where $x_q = q_c/q$ for $q > q_c$ [34].

6. Statistics of two-point conductances

So far, we have investigated properties of an open system. To define the two-terminal conductance g, one opens the system by attaching two leads. According to the Landauer–Büttiker formula, $g = \mathrm{Tr}\, t^{\dagger} t$, where t is the transmission matrix between the leads. In the framework of network models, the transmission matrix determining the two-point conductance between the edges e and e' has the form [16]

$$t = \langle e'|(1 - \mathcal{U}P)^{-1}\mathcal{U}|e\rangle \tag{72}$$

where $P = \mathbf{1} - |e\rangle\langle e| - |e'\rangle\langle e'|$ projects out the states on the edges e and e'.

The statistics of the two-point conductance $g(\mathbf{r}, \mathbf{r}')$ has been extensively studied, both analytically and numerically, for the conventional QH transition, exemplifying a localization transition with non-critical DOS. It was shown that the moments $\langle g^q(\mathbf{r}', \mathbf{r})\rangle$ obey a power-law scaling [16, 17, 39],

$$\langle g^q(\mathbf{r}, \mathbf{r}')\rangle \sim |\mathbf{r} - \mathbf{r}'|^{-X_q} \tag{73}$$

with a set of exponents X_q related to Δ_q [19, 20],

$$X_q = \begin{cases} \Delta_q + \Delta_{1-q} & q < 1/2 \\ 2\Delta_{1/2} & q > 1/2. \end{cases} \tag{74}$$

For the SQH critical point, only the average conductance $\langle g(e', e)\rangle$ has been considered previously. Gruzberg *et al* [10] found that

$$X_1 = 2x_\rho = \tfrac{1}{2}. \tag{75}$$

Beamond *et al* [13] used the mapping onto percolation to calculate $\langle g(e', e)\rangle$ at the band centre $\epsilon = 0$ ($z = 1$), with the result

$$\langle g(e', e)\rangle = 2P(e', e) \tag{76}$$

with $P(e', e)$ as defined in equation (33). Comparing (76) with (29), we see that $\langle g(e', e)\rangle$ is equal (up to the sign) to the diffusion propagator $\Pi(e', e) = \langle \mathrm{Tr}\, G_R(e', e; 1)G_A(e, e'; 1)\rangle$.

In this section, we will study statistical properties of $g(e', e)$ at the SQH transition. Note that though the definition of $\langle g(e', e)\rangle$ reminds us closely of that of the diffusion propagator $\Pi(e', e)$, the identical scaling of both quantities is not at all self-evident. In contrast, they scale differently at conventional localization transitions, as can be easily seen by comparing equations (73), (74) with (5). It is worthwhile to remind the reader of the physical reason for this difference (see also a related discussion in [16]). The product $\left\langle G_E^R(\mathbf{r}', \mathbf{r})G_E^A(\mathbf{r}, \mathbf{r}')\right\rangle$ has a meaning of the particle density (or, in an optical analogy, the radiation intensity) at a point $\mathbf{r}'$, induced by a source inserted into the system at a point $\mathbf{r}$. In an infinite system at criticality this quantity turns out to be infrared divergent: if a source is switched on at a time $t = 0$, the detected intensity will increase with time without saturation, since the radiation cannot propagate away fast enough. Therefore, in order to make $\langle G^R G^A \rangle$ finite, one needs to allow the propagating wave to get out of the system, i.e. to introduce absorption. One possibility is to make the absorption weak but uniform over the whole system, leading to $\left\langle G_{E+i\gamma}^R(\mathbf{r}', \mathbf{r})G_{E-i\gamma}^A(\mathbf{r}, \mathbf{r}')\right\rangle \equiv \Pi(\mathbf{r}', \mathbf{r}; 2i\gamma)$, which is the same as introducing a small uniform level broadening γ (or equivalently, a small frequency ω with an analytical continuation to the imaginary axis, $\omega = 2i\gamma$). Alternatively, one can allow for a particle to be absorbed at the points $\mathbf{r}$ and $\mathbf{r}'$ only, but with a probability of order unity, yielding the two-point conductance $g(\mathbf{r}', \mathbf{r})$. Clearly, the two definitions are essentially different (which is already obvious from the very fact that Π depends on γ, diverging in the limit $\gamma \to 0$, while g does not require any parameter such as γ and is bounded, $g \leqslant 1$). Therefore, different scaling behaviour of Π, equation (5) and $\langle g \rangle$, equation (73) is not surprising.

Returning to the SQH transition, we are thus naturally led to a question: why do Π and $\langle g \rangle$ scale identically in this case? The reason is that the zero-energy diffusion propagator $\Pi(e', e)$ is in fact defined at $\gamma = 0$ (i.e. there is no need to introduce absorption or a finite frequency to regularize it), see equations (32) and (58), (60). This can be traced back to the vanishing of DOS at $\epsilon = 0$. It is not a surprise that in this situation, when the absorption is irrelevant, $\Pi(e', e)$ and $\langle g(e', e) \rangle$ (which only differ in the way the absorption is incorporated) scale in the same way.

Let us consider now higher moments

$$\langle [\mathrm{Tr}\, G(e', e; e^{-\gamma}) G(e, e'; e^{\gamma})]^q \rangle.$$

Applying the consideration of section 4.3, we find that the absorption (γ) remains irrelevant provided

$$2q x_\rho + \Delta_{2q} > 0 \tag{77}$$

with the result

$$\langle [\mathrm{Tr}\, G(e', e; e^{-\gamma}) G(e, e'; e^{\gamma})]^q \rangle \sim r^{-2(q x_\rho + \Delta_q)}. \tag{78}$$

For the SQH case, condition (77) implies $q < 3/2$. (We make an assumption that our consideration, which is strictly speaking performed for integer q, remains valid for intermediate, non-integer values of q.) According to the above argument, $\langle g^q \rangle$ scales in this regime in the same way (78) so that (see also [23])

$$X_q = 2q x_\rho + 2\Delta_q \tag{79}$$

and, using $x_\rho = 1/4$ and equation (69),

$$X_q \simeq q(3 - q)/4. \tag{80}$$

Note that, in contrast to $\mathrm{Tr}\, GG$, the two-terminal conductance g is bounded from above, $g \leqslant 2$ (the factor two is due to spin summation and is not essential). Physically, it simply means that for such rare realizations when $\mathrm{Tr}\, GG$ is large, g is limited by the contact resistance. It follows that the exponent for $\langle g^q \rangle$ should be a non-decreasing function of q. In other words, the exponent X_q saturates after reaching its maximum at some q_0. We find from (80) $q_0 \simeq 3/2$; for larger q the exponent saturates at the value $X_{q \geqslant q_0} = X_{q_0} \simeq 9/16$ (these moments are determined by the probability to find $g \sim 1$).

Equation (80) implies, in particular, a normal distribution of $\ln g$ at $r \gg 1$ with the average $\langle \ln g(r) \rangle = -X_t \ln r$ and the variance $\mathrm{var}[\ln g(r)] = b \ln r$, where $X_t \simeq 3/4$ and $b \simeq 1/2$. These values correspond to the parabolic approximation (69); more accurate predictions can be obtained by using the numerical results for Δ_q,

$$X_t = X'_0 = 2x_\rho + 2\Delta'_0 = 2x_\rho + 2(\alpha_0 - 2) \simeq 0.774 \tag{81}$$

$$b = -X''_0 = -2\Delta''_0 \simeq 0.58 \tag{82}$$

(here a prime denotes the derivative with respect to q).

We now turn to a numerical study of the two-point conductance. While we did not attempt a high-precision numerical determination of the spectrum of corresponding exponents X_q (as presented in section 5.1 for the multifractal spectrum of wavefunctions), we have verified some of the key predictions of the above analytical considerations. Figure 7 illustrates evolution of the distribution function $\mathcal{P}(g)$ with the distance r between the contacts; it is seen that at sufficiently large r the distribution becomes log-normal as expected. In figure 8, we show the scaling of the average $\langle g \rangle$ and the typical $g_{\mathrm{typ}} = \exp\langle \ln g \rangle$ values of the two-point conductance, along with analogous quantities $\langle |G|^2 \rangle$ and $|G|^2_{\mathrm{typ}} = \exp\langle \ln |G|^2 \rangle$ for a
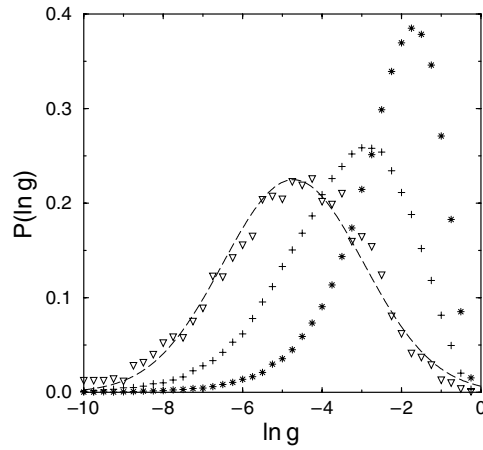
Figure 7. Distribution of the two-point conductance at three different distances between the contacts, $r = 5.7$ ($*$), 14.1 ($+$), 133 ($\triangledown$); the system size is $L = 196$. The dashed line indicates a log-normal fit with parameters $\langle \ln g \rangle = -4.72$ and $\mathrm{var}(\ln g) = 3.15$.
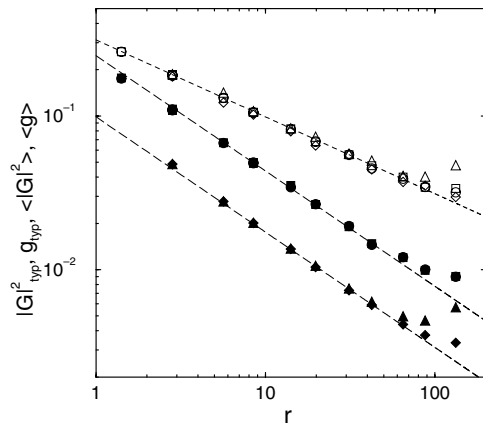

Figure 8. Scaling of the two-point conductance with distance r between the contacts: average value (empty symbols), $\langle g \rangle$, and typical value (full symbols), $g_{\mathrm{typ}} = \exp\langle \ln g \rangle$, in systems of sizes $L = 128$ ($\square$) and $L = 196$ ($\circ$). Also shown is the scaling of the two-point Green function, $\langle |G|^2 \rangle$ and $|G|^2_{\mathrm{typ}} = \exp\langle \ln |G|^2 \rangle$ ($L = 128$ ($\triangle$), $L = 196$ ($\diamond$)). The lines correspond to the $r^{-1/2}$ (dotted) and $r^{-3/4}$ (dashed) power laws. Deviations from power-law scaling at large values of r are due to the finite system size.

closed system, $|G|^2 \equiv -\mathrm{Tr}\, G(e', e; 1) G(e, e'; 1)$. For the average values, $\langle g \rangle$ and $\langle |G|^2 \rangle$, the numerics fully confirm the theoretical results (76), (29) telling us that both quantities scale as $r^{-1/2}$ and, moreover, are equal to each other. A non-trivial character of the equality $\langle g \rangle = \langle |G|^2 \rangle$ is well illustrated by the data for typical quantities: g_{typ} and $|G|^2_{\mathrm{typ}}$ are not equal. Nevertheless, they are found to share a common scaling: $g_{\mathrm{typ}}, |G|^2_{\mathrm{typ}} \sim r^{-X_t}$, confirming our arguments presented above. Furthermore, the numerically obtained value of the exponent, $X_t \simeq 3/4$, is in agreement with the theoretical prediction (81).

7. Summary

Let us summarize the main results of the paper.

1. We have extended the mapping of the SQH network model onto the classical percolation and calculated two- and three-point correlation functions at the SQH transition. This allowed us to determine analytically the fractal exponents Δ_2 and Δ_3 governing the scaling of the second and third moments of the wavefunction intensity, with the results $\Delta_2 \equiv -\eta = -1/4$ and $\Delta_3 = -3/4$.

2. We have performed a thorough numerical study of the multifractal spectrum Δ_q. The obtained spectrum is given with a good accuracy by the parabolic law (69), but shows clear deviations from parabolicity (figure 4).

3. Statistical properties of generalized inverse participation ratios P_q at the SQH transition are similar to those found earlier for other localization transitions. In particular, the distribution function $\mathcal{P}(P_q)$ becomes scale-invariant in the limit of large system size.

4. We have analysed statistics of the two-point conductance g at the localization transition with a critical density of states. Specifically, we have presented scaling arguments which link the exponents X_q governing the spatial decay of $\langle g^q \rangle$ to the wavefunction multifractality spectrum Δ_q (see equation (79)). This yields, in particular, for the typical conductance at the SQH critical point $g_{\text{typ}} \sim r^{-X_t}$ with $X_t \simeq 3/4$ (see equation (81) for a more accurate value), as confirmed by numerical simulations.

In recent years, considerable progress has been made in understanding the conformal field theories related to problems of two-dimensional fermions subject to quenched disorder [17, 18, 21–23, 32, 40–46]. In particular, a relation between the wavefunction multifractality in two-dimensional disordered systems and the operator content of corresponding conformal field theories has been discussed in a number of publications [18, 23, 32, 42]. It remains an open question whether the multifractal exponents Δ_q, X_q for the SQH transition can be computed by the conformal field theory methods. Note that our results are against the proposal of [23], where the result $\Delta_q = q(1 - q)/4$ was obtained. Apparently, this indicates that the theory considered in [23] and obtained [22] from a particular network model with fine-tuned couplings does not belong to the SQH universality class.

Acknowledgments

Appendix. Proofs of the mapping onto percolation

In section 4.1 two statements were formulated which allow us to calculate averaged products of two (section 4.1) and three (section 4.2) Green functions. Here we give some more details on the proofs of these statements. At the end of the appendix we will also explain why our calculation cannot be extended to products of $q \geqslant 4$ Green functions (and thus to higher moments of wavefunctions).

A.1. Statement 1

The first statement says that only paths visiting each node 0 or 2 times are to be considered. Its proof for the case of two-point functions was given in section 4.1. The analysis of the case
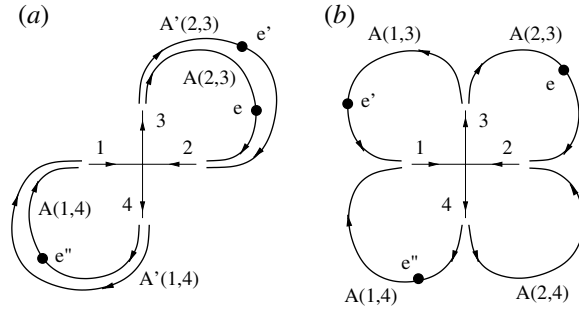
Figure 9. Configurations of paths for the correlation function (47) for a node visited four times.

of three-point functions (considered in section 4.2) goes along similar lines, and we present its brief outline only. In analogy with (22), we have to consider an expression of the type

$$\sum_{k_1,k_2,k_3=1}^{\infty} \langle \mathrm{Tr}\, B_1 U_f^{k_1} B_2 U_f^{k_2} B_3 U_f^{k_3} \rangle |A(f,f)|^{k_1+k_2+k_3} \tag{A1}$$

where k_i is the number of returns of the ith path ($i = 1, 2, 3$) to the edge f. Performing averaging over U_f as in (23), we cast (A1) into the following form:

$$\sum_{k_1,k_2,k_3=1}^{\infty} \left(b_1 c_{k_1+k_2+k_3} + b_2 c_{k_1+k_2-k_3} + b_3 c_{k_1+k_3-k_2} + b_4 c_{k_2+k_3-k_1} \right) |A(f,f)|^{k_1+k_2+k_3}. \tag{A2}$$

The first term in curly brackets is trivially zero in view of (19). To demonstrate that remaining terms give zero as well, we perform a summation over k_i at fixed $k = k_1 + k_2 + k_3$. Indeed, it is not difficult to show by a straightforward arithmetic that for an arbitrary k

$$\sum_{k_{1,2,3}=1,2,\dots;\, k_1+k_2+k_3=k} c_{k_1+k_2-k_3} = 0. \tag{A3}$$

Therefore, the sum (A2) is equal to zero, which completes the proof of the statement 1 for the three-point Green functions.

A.2. Statement 2

The second statement allows us to reduce the nodes visited four times to a superposition of contributions (i) and (ii) of figure 2, with the factors $\cos^2 \theta$ and $\sin^2 \theta$, respectively. We will give the proof for the (most non-trivial) case of a product of $q = 3$ Green functions; the proof for $q = 1$ and 2 is obtained in the same way. More specifically, we will consider the correlation function (47); the correlator (46) is treated analogously.

Each of three Green functions in (47) generates a sum over closed loops ($e \to e$, $e' \to e'$ and $e'' \to e''$, respectively). For a given lattice node, let us label the corresponding incoming edges as (1, 2) and the outgoing ones as (3, 4). We are considering a contribution of paths visiting this node in total four times. This generates four path segments starting each on one of the edges (3, 4) and ending on one of the edges (1, 2) and not passing through any of these edges. We are going to show that for any configuration of these four segments statement 2 holds. It is easy to see that there exist two essentially different types of such configurations (shown in figure 9); all others can be obtained by permutations of e, e' and e'', and/or by lattice symmetry operations.

Consider first the configuration (a) of figure 9. We have to sum over all ways to connect the four path segments by various configurations of scattering events at this node shown in figure 2. Specifically, only such connections are allowed which generate exactly three closed loops, each containing one of the edges e, e', and e''. There are three possibilities how this can be done, since the segment that does not contain any of the edges e, e', e'' can be connected in a loop with any of the remaining three. In one of these cases the configuration of paths at the considered node is of type (ii) of figure 2, in the two other cases it is of type (iii). We thus get the following contributions:

$$\langle \text{Tr}\, U_2 A(2, 3)U_3 \,\text{Tr}\, U_2 A'(2, 3)U_3 \text{Tr}\, U_1 A(1, 4)U_4 U_1 A'(1, 4)U_4\rangle \times s^4 \tag{A4}$$

$$\langle \text{Tr}\, U_2 A(2, 3)U_3 \,\text{Tr}\, U_1 A(1, 4)U_4 \,\text{Tr}\, U_2 A'(2, 3)U_3 U_1 A'(1, 4)U_4\rangle \times (-c^2 s^2) \tag{A5}$$

$$\langle \text{Tr}\, U_2 A'(2, 3)U_3 \,\text{Tr}\, U_1 A(1, 4)U_4 \,\text{Tr}\, U_2 A(2, 3)U_3 U_1 A'(1, 4)U_4\rangle \times (-c^2 s^2). \tag{A6}$$

Here $A(2, 3)$ is a sum over all paths from 3 to 2 passing through e, $A'(2, 3)$ is a sum over paths $3 \to e' \to 2$, $A(1, 4)$ is a sum over paths $4 \to e'' \to 1$ and $A'(1, 4)$ is a sum over paths $4 \to 1$ (figure 9(a)). Also, we have denoted $s = \sin\theta$ and $c = \cos\theta$.

To perform the integration over U_i, we use the following formulae of integration over $SU(2)$ matrices:

$$\langle \text{Tr}\, U V_1 \,\text{Tr}\, U V_2\rangle_U = \tfrac{1}{2}\text{Tr}\, V_1^\dagger V_2 \tag{A7}$$

$$\langle \text{Tr}\, U V_1 U V_2\rangle_U = -\tfrac{1}{2}\text{Tr}\, V_1^\dagger V_2 \tag{A8}$$

$$\langle \text{Tr}\, U V_1 U^\dagger V_2\rangle_U = \tfrac{1}{2}\text{Tr}\, V_1 \,\text{Tr}\, V_2. \tag{A9}$$

Here matrices $V_{1,2}$ are assumed to be of the form $V_i = |V_i|\tilde{V}_i$, where $\tilde{V}_i \in SU(2)$ and $|V_i|$ is a real number (we recall that $A(i, j)$ are exactly of this type, see section 4.1).

Applying repeatedly the rules (A7)–(A9), we perform integration over all matrices U_i ($i = 1, \ldots, 4$) in equations (A4)–(A6). We then find that all three contributions (A4)–(A6) are proportional to $\text{Tr}\, A^\dagger(2, 3)A'(2, 3) \,\text{Tr}\, A^\dagger(1, 4)A'(1, 4)$, with coefficients $-\tfrac{1}{4}s^4$, $-\tfrac{1}{8}c^2 s^2$ and $-\tfrac{1}{8}c^2 s^2$, respectively. The total coefficient is therefore

$$-\tfrac{1}{4}s^4 - \tfrac{1}{8}c^2 s^2 - \tfrac{1}{8}c^2 s^2 = -\tfrac{1}{4}s^2. \tag{A10}$$

We see that the same result would be obtained if we assign the weight s^2 to the first contribution (which is of type (ii) of figure 2) and discard the remaining two terms (which are of type (iii)). This establishes the validity of the statement 2 with respect to the configuration (a) of figure 9.

Configuration (b) of figure 9 is analysed along the same lines. We have again three contributions, one of type (ii) of figure 2 and two of type (iii),

$$\langle \text{Tr}\, U_2 A(2, 3)U_3 \,\text{Tr}\, U_1 A(1, 4)U_4 \,\text{Tr}\, U_1 A(1, 3)U_3 U_2 A(2, 4)U_4\rangle \times s^4 \tag{A11}$$

$$\langle \text{Tr}\, U_2 A(2, 3)U_3 \,\text{Tr}\, U_1 A(1, 3)U_3 \,\text{Tr}\, U_1 A(1, 4)U_4 U_2 A(2, 4)U_4\rangle \times (-c^2 s^2) \tag{A12}$$

$$\langle \text{Tr}\, U_1 A(1, 3)U_3 \,\text{Tr}\, U_1 A(1, 4)U_4 \,\text{Tr}\, U_2 A(2, 3)U_3 U_2 A(2, 4)U_4\rangle \times (-c^2 s^2). \tag{A13}$$

After integration over U_i according to the rules (A7)–(A9), they all produce an identical structure, $\text{Tr}\, A^\dagger(2, 3)A(2, 4)A^\dagger(1, 4)A(1, 3)$, with the coefficients $\tfrac{1}{4}s^4$, $\tfrac{1}{8}c^2 s^2$ and $\tfrac{1}{8}c^2 s^2$, respectively. Again, retaining only the (ii)-type contribution (A11) and assigning the weight s^2 to it, we would obtain the same result. This completes the proof of statement 2 for the three-point correlation function (47).

A.3. What about q > 3?

A natural question is whether the present approach can be generalized to higher-order correlations of wavefunctions governed by multifractal exponents Δ_q with $q > 3$. The answer is negative. In fact, neither of statements 1 and 2 apply (or, in a more careful formulation, our proofs fail) for $q \geqslant 4$, as we are going to explain in brief. Concerning statement 1, consider a generalization of the expression (A1) to $q = 4$, and choose $k \equiv k_1 + k_2 + k_3 + k_4 = 4$. Obviously, there is just one such term (all $k_i = 1$) in the sum, and it is easy to see that it is generically non-zero. Therefore, no cancellation of terms with $k > 2$ happens in this case, i.e. statement 1 does not work. Turning to statement 2, consider, e.g., a correlation function $\tilde{D}(e, e', e'', e'''; \gamma)$ analogous to (47) but containing a product of four traces of Green functions. Trying to prove statement 2, we will then have to consider path configurations very similar to those shown in figure 9 but with all four paths containing one of the edges e, e', e'', or e'''. At the next step the paths should be connected via the scattering processes at the node—this time to generate four closed loops. However, for each of the configurations shown in figure 9 there is only one way to do this, so that only one contribution will arise in place of three terms (A4)–(A6) or (A11)–(A13). Clearly, statement 2 is not valid in this situation. Therefore, the mapping onto the classical percolation is not applicable for higher moments, $q > 3$. This is in correspondence with the fact that $q = 3$ separates two regimes of qualitatively different behaviour of correlation functions, as discussed in section 4.3.

References

[1] Wigner E P 1951 *Ann. Math.* **53** 36
    Wigner E P 1958 *Ann. Math.* **67** 325
[2] Dyson F J 1962 *J. Math. Phys.* **3** 140, 1199
[3] Guhr T, Müller-Groeling A and Weidenmüller H A 1998 *Phys. Rep.* **299** 189
[4] Verbaarschot J J M 1994 *Phys. Rev. Lett.* **72** 2531
[5] Gade R 1993 *Nucl. Phys.* B **398** 499
[6] Altland A and Zirnbauer M R 1997 *Phys. Rev.* B **55** 1142
[7] Zirnbauer M R 1996 *J. Math. Phys.* **37** 4986
[8] Kagalovsky V, Horovitz B, Avishai Y and Chalker J T 1999 *Phys. Rev. Lett.* **82** 3516
[9] Senthil T, Marston J B and Fisher M P A 1999 *Phys. Rev.* B **60** 4245
[10] Gruzberg I A, Ludwig A W W and Read N 1999 *Phys. Rev. Lett.* **82** 4524
[11] Laughlin R B 1998 *Phys. Rev. Lett.* **80** 5188
    Movshovich R, Hubbard M A, Salamon M B, Balatsky A V, Yoshizaki R, Sarrao J L and Jaime M 1998 *Phys. Rev. Lett.* **80** 1968
    Balatsky A V 1998 *Phys. Rev. Lett.* **80** 1972
    Balatsky A V 2000 *Phys. Rev.* B **61** 6940
[12] Cardy J 2000 *Phys. Rev. Lett.* **84** 3507
[13] Beamond E J, Cardy J and Chalker J T 2002 *Phys. Rev.* B **65** 214301
[14] Huckestein B 1995 *Rev. Mod. Phys.* **67** 357
[15] Janssen M 1998 *Phys. Rep.* **295** 1
[16] Janssen M, Metzler M and Zirnbauer M R 1999 *Phys. Rev.* B **59** 15836
[17] Zirnbauer M R 1999 *Preprint* hep-th/9905054v2
[18] Bhaseen M J, Kogan I I, Soloviev O A, Taniguchi N and Tsvelik A M 2000 *Nucl. Phys.* B **580** 688
    Tsvelik A M 2001 *Preprint* cond-mat/0112008
[19] Klesse R and Zirnbauer M R 2001 *Phys. Rev. Lett.* **86** 2094
[20] Evers F, Mildenberger A and Mirlin A D 2001 *Phys. Rev.* B **64** 241303(R)
[21] Fendley P and Konik R M 2000 *Phys. Rev.* B **62** 9359
    Fendley P 2000 *Preprint* cond-mat/0006360
[22] Bernard D and LeClair A 2001 *Phys. Rev.* B **64** 045306
[23] Bernard D and LeClair A 2002 *Nucl. Phys.* B **628** 442
[24] Evers F, Mildenberger A and Mirlin A D 2002 *Preprint* cond-mat/0203134

[25] Mirlin A D 2000 *Phys. Rep.* **326** 259
[26] Chalker J T and Coddington P D 1988 *J. Phys. C: Solid State Phys.* **21** 2665
[27] Saleur H and Duplantier B 1987 *Phys. Rev. Lett.* **58** 2325
[28] Moore J E 2002 *Phys. Rev.* B **65** 241309
[29] Wegner F 1980 *Z. Phys.* B **36** 209
[30] Wegner F 1985 *Localisation and Metal Insulator Transitions* ed H Fritzsche and D Adler (New York: Plenum) p 337
[31] Duplantier B and Ludwig A W W 1991 *Phys. Rev. Lett.* **66** 247
[32] Mudry C, Chamon C and Wen X-G 1996 *Nucl. Phys.* B **466** 383
[33] Demmel J W, Eisenstat S C, Gilbert J R, Li X Y S and Liu J W H 1999 *SIAM J. Matrix Anal. Appl.* **20** 720
     Lehoucq R B, Sorensen D and Yang C 1998 *ARPACK Users Guide* (Philadelphia, PA: SIAM)
[34] Evers F and Mirlin A D 2000 *Phys. Rev. Lett.* **84** 3690
     Mirlin A D and Evers F 2000 *Phys. Rev.* B **62** 7920
[35] Cuevas E, Ortuño M, Gasparian V and Pérez-Garrido A 2002 *Phys. Rev. Lett.* **88** 016401
[36] Mildenberger A, Evers F and Mirlin A D 2002 *Phys. Rev.* B **66** 033109
[37] Cuevas E 2002 *Preprint* cond-mat/0204197
[38] Fyodorov Y V and Mirlin A D 1995 *Phys. Rev.* B **51** 13403
[39] Zirnbauer M R 1994 *Ann. Phys., Lpz* **3** 513
[40] Ludwig A W W, Fisher M P A, Shankar R and Grinstein G 1994 *Phys. Rev.* B **50** 7526
[41] Nersesyan A A, Tsvelik A M and Wenger F 1995 *Nucl. Phys.* B **438** 561
[42] Caux J S, Taniguchi N and Tsvelik A M 1998 *Phys. Rev. Lett.* **80** 1276
     Caux J S, Taniguchi N and Tsvelik A M 1998 *Nucl. Phys.* B **525** 621
     Caux J S 1998 *Phys. Rev. Lett.* **81** 4196
[43] Gurarie V 1999 *Nucl. Phys.* B **546** 765
[44] Read N and Saleur H 2001 *Nucl. Phys.* B **613** 409
[45] Altland A, Simons B D and Zirnbauer M R 2002 *Phys. Rep.* **359** 283
[46] Gurarie V and Ludwig A W W 2002 *J. Phys. A: Math. Gen.* **35** L377